

Dust outflows from starburst galaxies

P.B. Alton, J.I. Davies, and S. Bianchi

Department of Physics and Astronomy, University of Wales, P.O. Box 913, Cardiff, CF2 3YB, UK

Received 11 September 1998 / Accepted 2 December 1998

Abstract. We present submillimeter SCUBA images of the nearby, starburst galaxies NGC 253, NGC 4631 and M82 (primarily at wavelengths of 450 and 850 μm). The edge-on orientation of our targets, in conjunction with the resolution of the instrument (15'' FWHM at 850 μm), allows us to probe the optically-obscured centre and resolve the minor-axis superwind from the main disk. For NGC 253 and M82, we detect a bright source, a few hundred parsec in diameter, which corresponds to the central starburst. In the case of M82, the bi-lobal nature of the central source is suggestive of a torus or ring.

We confirm the existence of a dust outflow along the minor axis of M82 and make a similar (but somewhat more tentative report) for the other two galaxies NGC 253 and NGC 4631. The scale-size of the ‘vertical’ features is 0.7–1.2 kpc. A mass of $10^{6-7} M_{\odot}$ is inferred for the outflowing grains in M82. We conclude that this amount of grain material could either have accrued from an inflow along the disk (e.g. a bar) or, if the lower mass limit applies, have been synthesized by massive stars in the starburst. The ejected grains are probably travelling close to the escape velocity of the host galaxy and assuming, hypothetically, that they *do* manage to breach the halo, we expect superwinds to expel up to 10% of the dust residing in interstellar disks into the intergalactic medium.

Key words: ISM: dust, extinction – galaxies: active – galaxies: intergalactic medium – galaxies: jets – galaxies: starburst – infrared: galaxies

1. Introduction

One of the most outstanding legacies of the Infrared Astronomical Satellite (IRAS) mission was the revelation that many more galaxies than previously thought undergo, at some point in their history, an intensive period of star formation (probably 10–50% of L_{\star} galaxies; Soifer et al. 1987). This *starburst* phase, which typically lasts no more than $\sim 10^8$ years (Leitherer 1993; Rieke et al. 1985), can often remain inconspicuous at optical wavelengths due to encircling swathes of optically thick gas (Sanders & Mirabel 1996). However, by the same token, the intense radiation emitted by the newly-formed stars is reprocessed by dust

grains to produce a bright, far-infrared (FIR) flux. Indeed, a high FIR-to-blue luminosity ratio is usually taken to be diagnostic of starburst activity (Soifer et al. 1987, Heckman et al. 1990).

The starburst phenomenon leaves spectacular traces on the interstellar medium (ISM) of the host galaxy. Supernova explosions and energetic stellar winds accelerate a hot plasma along the minor axis which subsequently emits copious X-rays and radio synchrotron radiation (Chevalier & Clegg 1985). The path of this outflow – or *superwind* as it has become known – is most evident in the $H\alpha$ ($\lambda 6584 \text{ \AA}$) line. As the superwind expands through the halo it impinges on denser, ambient gas producing a diffuse network of kpc-scale emission-line filaments (see Heckman et al. 1990 for a review of this effect). In addition, the outflowing plasma appears capable, by some as yet poorly-understood mechanism, of entraining neutral material to a height of at least several kpc above the disk. Both molecular and atomic gas have been observed moving outwards at velocities of several hundred km s^{-1} and prominent dust outflows (or chimneys) have been detected in B-I colour images of a few nearby, starburst galaxies (Nakai et al. 1987; Phillips 1993; Koribalski et al. 1992, Ichikawa et al. 1994). ‘Displaced’ grains have also been detected using optical imaging polarimetry – a technique sensitive to scattered, polarized light. In this case, dust clouds rising several kpc above the disk behave as giant reflection nebulae scattering light from the starburst towards the observer (Scarrott et al. 1991; Alton et al. 1994; Scarrott et al. 1993).

The possibility that galaxies may eject dusty, metal-rich gas into their halos (and potentially beyond into the intercluster medium) is more than just an intriguing sideline. Such a process will play an integral part in galactic chemical evolution acting as a sink for heavy elements (Eales & Edmunds 1996; Edmunds 1996). Moreover, given that we effectively see the distant Universe through a screen of foreground galaxies and clusters, it is precisely those tenuous (but expansive) dust clouds which are situated *between* galaxies that are most effective in attenuating and reddening light from background objects (Heisler & Ostriker 1988; Masci 1998). Confirmation of a dusty intergalactic medium may compel us to re-interpret high-redshift photometry and its implied cosmic star formation rates (Madau et al. 1998) and cause us to revise our understanding of quasar absorption systems (Malhotra 1997).

Send offprint requests to: P.B. Alton (paul.alton@astro.cf.ac.uk)

Table 1. Basic properties of the observed starburst galaxies. Right ascension and declination are taken from the RC3 (de Vaucouleurs et al. 1991) [note that the nuclear position is often poorly defined for edge-on galaxies due to severe dust obscuration]. The total flux densities F_{60} and F_{100} are derived from IRAS maps discussed in Sect. 2.4. L_{FIR}/L_B is the FIR-to-blue luminosity ratio as defined by de Jong et al. (1984) (L_{FIR} is the flux, in Wm^{-2} , between $40\ \mu\text{m}$ and $120\ \mu\text{m}$ and L_B is the ‘blue luminosity’, also in Wm^{-2} , given by $\nu F_\nu[\lambda = 0.43\ \mu]$.) As a point of reference, the typical L_{FIR}/L_B for quiescent galaxies is 0.3 (Alton et al. 1998; Soifer et al. 1987). In the penultimate column, we adopt the distance D as the most commonly used value in the literature. Finally, we show the major axis size, D_{25} , as tabulated in the RC3.

Galaxy	R.A. (1950)	Dec. (1950)	F_{60} (Jy)	F_{100} (Jy)	L_{FIR}/L_B	D (Mpc)	D_{25} (arcmin)
NGC 253	00 45 05.7	−25 33 40	1055	1457	2.58	2.5	27.5
M82	09 51 45.3	+69 55 11	1500	1510	8.76	3.3	11.2
NGC 4631	12 39 41.5	+32 48 54	100.2	179.6	1.06	8.1	15.5

In this paper, we examine 3 nearby galaxies which are undergoing a period of starburst activity. Submillimeter (submm) imaging is employed to (i) reveal the distribution of dust close to the starburst and (ii) investigate the hypothesis that large amounts of dust and metals are being expelled from the disk. Finally, we attempt to relate these observations to issues such as intercluster enrichment by dust grains.

2. Observations

2.1. Object selection

Our targets were chosen on the basis of proximity and near edge-on orientation. In this way we ensured that the minor axis was most clearly resolved from the disk. A list was compiled of nearby, edge-on galaxies known, from the literature, to be experiencing intense starburst activity and noted, observationally, as having a starburst-driven superwind (usually through means of $\text{H}\alpha$ emission-line studies). Of these objects, we selected the 3 closest galaxies which were readily observable from the James Clerk Maxwell Telescope (JCMT; declination 20°). These targets are listed in Table 1 along with their salient properties.

Due to their proximity, the objects in Table 1 have all undergone significant previous investigation. NGC 4631 is known to possess a dramatic series of $\text{H}\alpha$ ‘spurs’ which rise 16 kpc above and below the disk (Donahue et al. 1995). Vigorous star formation appears to be particularly prevalent in the inner $3'$ of this galaxy but there is also substantial activity on the east side of the disk (Rand et al. 1992). X-ray observations with ROSAT, plus radio continuum mapping, have revealed a diffuse halo of hot, ionized gas extending to at least 8 kpc above the midplane (Wang et al. 1995; Hummel & Dettmar 1990). Similarly, NGC 253 is characterized by a synchrotron-emitting halo and an outflow of hot X-ray gas from the nuclear region (Carilli et al. 1992; Fabbiano & Trinchieri 1984). Sofue et al. (1994) describe NGC 253 as a ‘boiling disk’ in which numerous thin dust streamers extend up to 2 kpc into the halo. These are driven by intense, recent star formation – both at the centre and along the spiral arms. In the past, M82 has been labelled *the archetypal* starburst galaxy and has been subject to numerous multi-wavelength studies (particular in $\text{H}\alpha$ where the galaxy takes on an ‘explosive’ appearance along its minor axis; McCarthy et al.

1987, McKeith et al. 1995. See also Bregman et al. 1995 and Telesco 1988 for more general references). Its purported status as the starburst paradigm is somewhat misleading – M82, with a D_{25} size of 11 kpc, is considerable smaller than most starburst galaxies. In addition, M82 possesses only a moderate global FIR luminosity ($2 \times 10^{10} L_\odot$; akin to our own Galaxy), although this energy, as we shall see, emanates almost exclusively from a very active region in the central kiloparsec.

2.2. Submillimeter observations

All three of our targets were observed in service mode between August and October 1997 at the James Clerk Maxwell Telescope (JCMT). The Submillimeter Common User Bolometer Array (SCUBA) is mounted at the Nasmyth focus of the telescope and its chief mode of operation is to provide simultaneous imaging at 450 and $850\ \mu\text{m}$ for a region of sky $2.3'$ in diameter. The short-wave array ($450\ \mu\text{m}$) consists of 91 bolometers (HPBW= $7.5''$) whilst the longwave array ($850\ \mu\text{m}$) is composed of 37 elements (HPBW= $14.7''$). In order to provide fully sampled images, the secondary mirror moves in a 64-step jiggle pattern with the integration time lasting 1 second at each position. At the same time, the secondary mirror chops at 7 Hz so as to remove the reference (sky) emission. After 16 steps of the jiggle pattern, the telescope nods in order to allow for slowly varying sky gradients. For all our targets, we used a chop throw of $3'$ perpendicular to the major axis. In addition to 450 and $850\ \mu\text{m}$ imaging, M82 was also observed with the array operating at 350 and $750\ \mu\text{m}$. Although the instrument is less sensitive at these wavelengths, M82 was deemed sufficiently bright to warrant these additional observations.

After each hour of observing, the telescope pointing was checked against a bright point source and skydip measurements were carried out to determine the atmospheric transparency according to elevation. The pointing stability was $< 5''$ and the zenith opacity was typically 0.24 at $850\ \mu\text{m}$ (1.5 at $450\ \mu\text{m}$). During each night, Uranus was mapped at least once in order to calibrate our images and determine the beam shape. The SCUBA beam has moderate error lobes (especially at $450\ \mu\text{m}$) and, since our targets are extended sources, we corrected the calibration in order to take account of emission outside the central beam. The measured HPBW of the central beam is $9''$ at

Table 2. Synopsis of SCUBA observations. *R.A.* and *Dec.* refer to the centre of the instrument’s field of view and define the origin for the maps in Fig. 1. T_{exp} is the exposure time for each bolometer in the array. The last column shows the 1σ noise level in the final, unsmoothed map.

Galaxy	Image centre		wavelength μm	T_{exp} (sec)	Beamsize (FWHM) (arcsec)	1σ mJy/beam
	R.A. (1950)	Dec. (1950)				
NGC 253	00 45 06.0	−25 33 40	450	2560	9	77
			850	2560	15	7
M82	09 51 43.6	+69 55 00	350	640	8	158
			450	1280	9	48
			750	640	14	17
			850	1280	15	10
NGC 4631	12 39 39.8	+32 48 48	450	1920	9	17
			850	1920	15	5

450 μm and 15'' at 850 μm . We estimate an error of 10% and 25% in the calibration at 850 μm and 450 μm respectively.

The dedicated SCUBA software package, SURF, was used to clean, flatfield and calibrate the images according to atmospheric attenuation (Jenness 1997). SURF also facilitates a reduction in the final image noise by compensating for spatially correlated sky emission across the field of view. Table 2 summarizes the on-source exposure time for each target and our achieved signal-to-noise in the final images.

2.3. Optical images

To compare with our submm maps we obtained, on request, optical data for our targets from the Isaac Newton Group (ING) archive, Cambridge. For M82, 3 frames taken at the 1.0-m Jakobus Kapteyn Telescope (JKT) using a TEK4 1024×1024 chip, gave a combined exposure of 780 seconds in B. Similarly, 2 frames of NGC 253, using the same instrumental setup, gave a total B-band exposure time of 1800 sec. Finally, 3 I-band frames of NGC 4631, taken with a EEV5 1242×1152 chip (also at the JKT), gave a total exposure time of 360 sec for this object.

The CCD data were reduced in the standard manner using the STARLINK software package CCDPACK to perform debiasing, flatfielding and sky subtraction etc. To register the final optical images with the corresponding SCUBA map, astrometry was carried out by means of Digitized Sky Survey (DSS) data and the Hubble Space Telescope (HST) guide star catalogue. Positions in the HST catalogue were used to astrometrically calibrate a DSS image of each object (which covers a larger part of the sky than our own image). Then the calibrated DSS image was registered with our own CCD data. We estimate that the positional calibration of our final optical images is accurate to 1'' (whilst the positional accuracy of our final SCUBA images is good to 3'').

2.4. High resolution IRAS data

Resolution-enhanced IRAS images at 12, 25, 60 and 100 μm (known as *HiRes*) were obtained for our SCUBA targets upon request from the Infrared Processing and Analysis Center at Caltech (IPAC). IPAC uses modelled responses of the 62 rect-

angular survey detectors in order to enhance the resolution of the survey data. For example, the pre-enhancement resolution at 60 and 100 μm is 3–5' FWHM, whereas after processing we obtain images with $\sim 1'$ resolution (see Rice 1993 for an in-depth discussion of this technique). The HiRes data for NGC 253 and NGC 4631 have already been presented and discussed elsewhere (Alton et al. 1998a). In both cases, a bright, unresolved FIR source located near the nucleus dominates emission from the disk (believed to be the starburst). Similarly, HiRes images of M82 show a bright point-like source at the centre and relatively little emission from the rest of the disk. Spatial information is constrained to 1' for these data (equivalent to 1–2 kpc) but our SCUBA images, with a beamsize of 9–15'', will resolve this region with ease.

3. Results

In Fig. 1, we show optical and submm maps of the three starburst galaxies M82, NGC 4631 and NGC 253. The submm continuum arises from dust grains heated by the stellar radiation field (the contribution from free-free electrons is $< 10\%$ at 850 μm and even less at 450 μm ; Smith et al. 1990). In general, since the 450 μm data show a similar morphology to the 850 μm data, we display only the latter which has a far better signal-to-noise. In each case, we also reproduce a contour map of the corresponding beam so that a comparison can be made between extended structure detected from the object and the shape of the PSF. In the following sections, maps for each of the starburst objects are discussed in turn.

3.1. M82

In the submm regime, M82 exhibits a double lobe structure at its centre and a network of filaments extending along the minor axis. In fact, despite the object’s near edge-on orientation, the contours in Fig. 1 are surprisingly circular, extending almost as far along the minor axis as they do along the disk. The central surface brightness at 850 μm is $1.4 \pm 0.14 \text{ Jy}/15'' \text{ beam}$ ($3.7 \pm 0.9 \text{ Jy}/9'' \text{ beam}$ at 450 μm) which is more than an order of magnitude brighter than any emission outside the central 1.2 kpc of the disk. This is consistent with IRAS (HiRes) images of M82

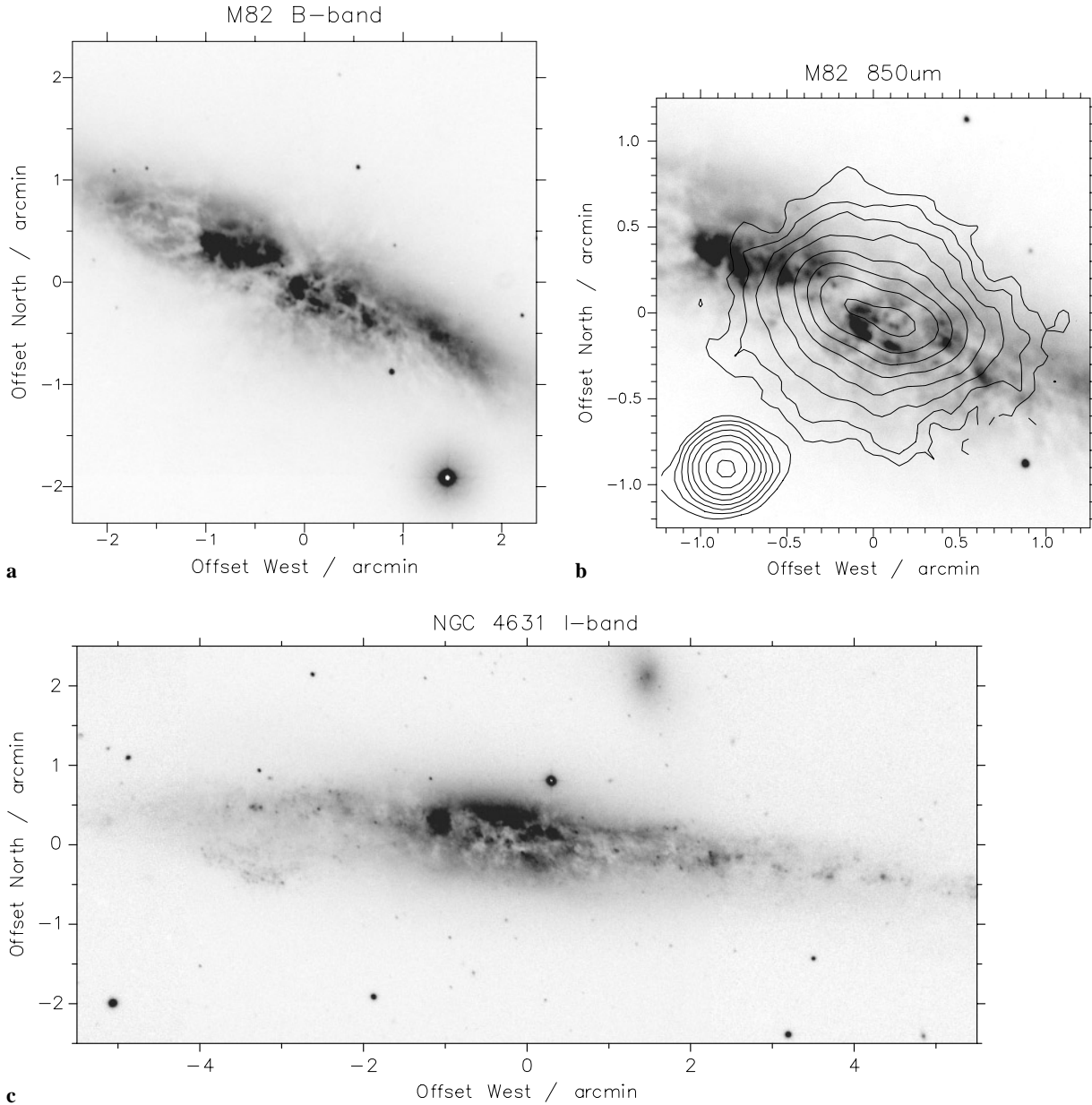


Fig. 1a–f. SCUBA observations of the starburst galaxies M82, NGC 4631 and NGC 253. In **a**, **c**, **e** we show an optical image of each galaxy whilst in **b**, **d**, **f** 850 μm contours are overlaid onto the central $3'$ region. For both these figures and Figs. 2 and 4, we label the axes as offsets from the centre of the instrument’s field of view (recorded in Table 2). The lowest contour is approximately 5σ (50, 23 and 44 mJy/ $15''$ beam for M82, NGC 4631 and NGC 253 respectively) and the separation between isophotes is 0.3 mag for NGC 4631 and 0.5 mag for M82 and NGC 253. Using the same contour interval, we reproduce, in each case, a map of the SCUBA beam at the bottom-left of the submm figure. The contour map for NGC 253 is also reproduced as a greyscale image in Fig. 2 in order to clarify the distribution of low and high surface brightness regions.

which simply show a point-like source at 60 μm , equivalent to $\approx 1'$ (900 pc) FWHM (Sect. 2.4).

The detection of a central, double-lobed source has been noted by previous submm/mm observers of M82 (see in particular the diffraction-limited 450 μm map produced by Hughes et al. 1994). The two maxima are separated by $16 \pm 2''$ (250 pc) at both 850 μm and 450 μm , and are symmetrically situated either side of the 2.2 μm (dynamical) centre of the galaxy (09h 51

43.5, 69° 55 00.7 (1950); Dietz et al. 1986). The toroidal nature of the starburst has been known about for some time (Telesco 1988). Bi-lobal structure, attributable to limb-brightening from an edge-on torus, has been observed in $\text{H}\alpha$ (McCarthy et al. 1987), mid-IR (Achtermann & Lacy 1995) and molecular gas (Nakai et al. 1987). We concur with Hughes et al. (1994) who assert that the submm torus encloses the mid-IR torus (10'' diameter) but is, at the same time, itself surrounded by a ring of

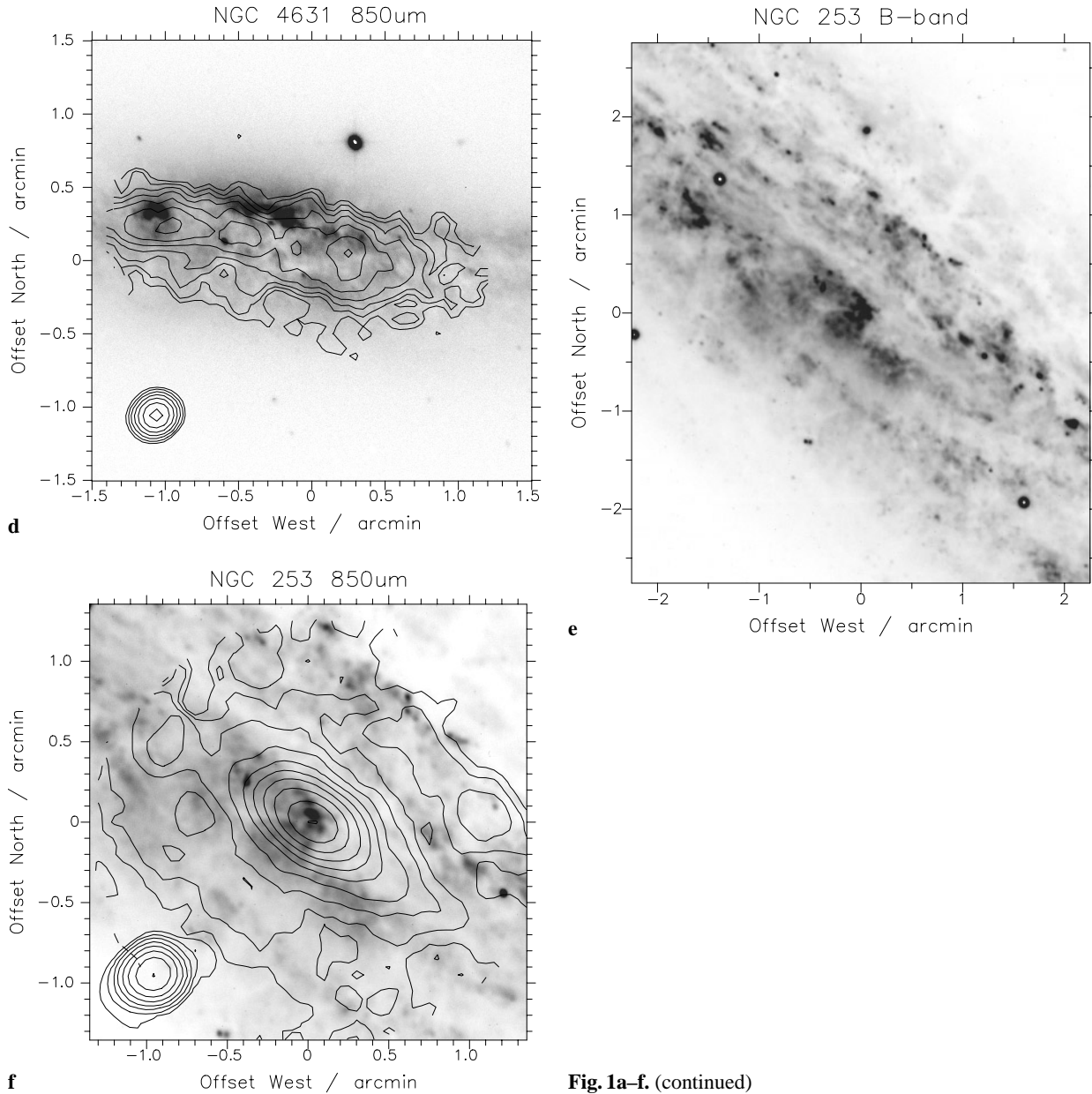


Fig. 1a–f. (continued)

molecular gas (diameter $26''$). It seems likely that the hot dust, giving rise to the mid-IR emission, traces the most recent star-forming activity as it propagates outwards through the dense gas surrounding the nucleus. Indeed, in spite of severe line-of-sight obscuration, HST images have revealed the presence of over 100 “super-starclusters” interior to the gas torus in question (O’Connell et al. 1995). The peak submm emission, on the other hand, occurs at a ‘compromise’ location between the radiation sources (young stars) and the greatest concentration of dust (the gas ring).

We detect submm emission up to at least $50''$ along the minor axis of M82. Assuming a tilt of 83° for the disk (Lynds & Savage 1963; de Vaucouleurs et al. 1991), we infer that dust grains have escaped to at least a z -height of 800 pc. Spurs of cool dust emission have also been recorded at 2mm, $450 \mu\text{m}$ and 1.3mm but not

to such large z -heights, or with as much sensitivity, as the current observations. The presence of dust ‘above’ the disk of M82 is beyond doubt – dust streamers splaying along the minor axis are evident in optical images (Fig. 1; see also the unsharp-mask image in Fig. 4) and grains have also been detected by means of scattered light (Scarrott et al. 1991 and references therein). Spurs of molecular gas have also been discovered along the minor axis, extending from the gas torus mentioned earlier to over 0.5 kpc above the disk (Nakai et al. 1987; Loiseau et al. 1990). Hughes et al. (1994) claim that the submm extensions in their $450 \mu\text{m}$ map correlate with the molecular spurs in such a way that the latter appear to collimate the grains as they leave the disk. Our own observations, which are much more sensitive and hence cover a larger part of the minor axis, show less evidence of a collimating effect or a “pile-up” of dust near the molec-

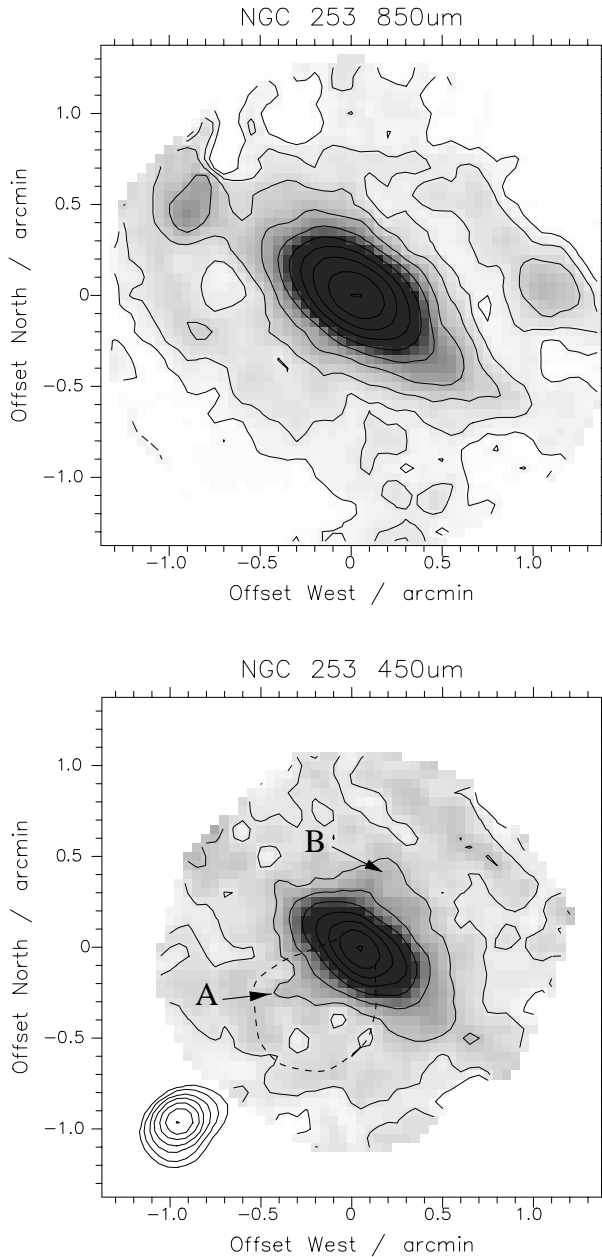


Fig. 2. Inverse greyscale images of NGC 253 at 850 and 450 μm . The 450 μm data have been smoothed to approximately the same resolution as the 850 μm image (15'' FWHM) for comparative purposes. Both images are contoured at 0.5 mag intervals, starting from 230 mJy/15'' beam at 450 μm and 44 mJy/15'' beam at 850 μm (5 and 6 σ respectively). The regions 'A' and 'B' in the lower image correspond to areas of outflow along the minor axis. The dashed line delineates the superwind gas previously detected in X-rays (see text for details).

ular outflow (although, otherwise, they broadly agree with the Hughes et al. data).

3.2. NGC 4631

In contrast to the compact torus structure observed at the centre of M82, SCUBA maps of NGC 4631 reveal several

'hot-spots' separated by one or more kpc. The picture that emerges is a galaxy which is less dominated by circum-nuclear star-formation and, indeed, previous observations in the H α emission-line have shown that about $\frac{2}{3}$ of the disk is undergoing enhanced star-formation (Rand et al. 1992). The most active region, associated with the outflow of X-ray gas (Fabbiano & Trinchieri 1984) and the origin of extensive H α filaments in the halo, is the inner 3' covered by our SCUBA map.

The submm exhibits numerous extensions away from the midplane; from this we infer that dust extends to a z-height of $\geq 30''$ (1.2 kpc). Images of NGC 4631 at 1.3mm exhibit similar extra-planar structures (Braine et al. 1995) but we cannot confirm the reality of the most southerly extension in the Braine et al. map (travelling up to 2.1 kpc away from the disk). The lowest contour in the Braine et al. map is barely 2 σ and, therefore, their most southerly filament must be considered doubtful. By contrast, the extraplanar structures evident in Fig. 1 are at least 5 σ and manifest themselves in each of the 'composite' jiggle maps making up the final image (as well as being present at both 450 and 850 μm). Notably, the submm filaments in Fig. 1 are *not* always positionally coincident with 'vertical' extinction features evident in optical images of NGC 4631 (Fig. 1). This is not surprising given that the latter arise chiefly from optically thick material on the near side of the disk whereas submm emission, being optically thin, probes the whole line-of-sight.

3.3. NGC 253

Our submm maps of NGC 253 show a bright, central source and fainter emission associated with the spiral dust lanes. The central source has a FWHM size of 21'' \times 6.5'' (250 pc \times 80 pc), which is comparable to the size of the starburst in M82, but does not appear to possess a toroidal structure. The central surface brightness is an order of magnitude greater than any other part of the disk which explains why a dominant point source was detected by the IRAS (HiRes) 1' beam (Sect. 2.4). A ring or torus of molecular gas has been discovered around the nucleus of NGC 253 (Mauersberger et al. 1996; Israel et al. 1995) which is very similar both in real size and in *apparent* size to that observed in M82. Accordingly, if recent star formation were concentrated on the inner surface of this molecular ring, we would expect to find a bi-lobal morphology similar to that detected in M82. Since this is not the case, it follows that star-forming activity may *not* always routinely propagate outwards from the centre of the starburst galaxy (consuming the surrounding molecular gas) as has been proposed by some authors (Telesco et al. 1993; Baum et al. 1993).

The inclination of NGC 253 (78 $^\circ$; Pence 1981) is less amenable than NGC 4631 or M82 to the detection of minor axis outflows. A bubble of shocked, emission-line gas has, however, been identified by McCarthy et al. (1987) at a position angle of $\simeq 140^\circ$ from the nucleus. In addition, Fabbiano & Trinchieri (1984) have discovered an outflow of hot, X-ray gas (the superwind) extending for about 45–60'' (~ 700 pc) in the same direction. The 850 μm map in Fig. 1 shows a slight extension at the same position angle as the purported outflow but it is not

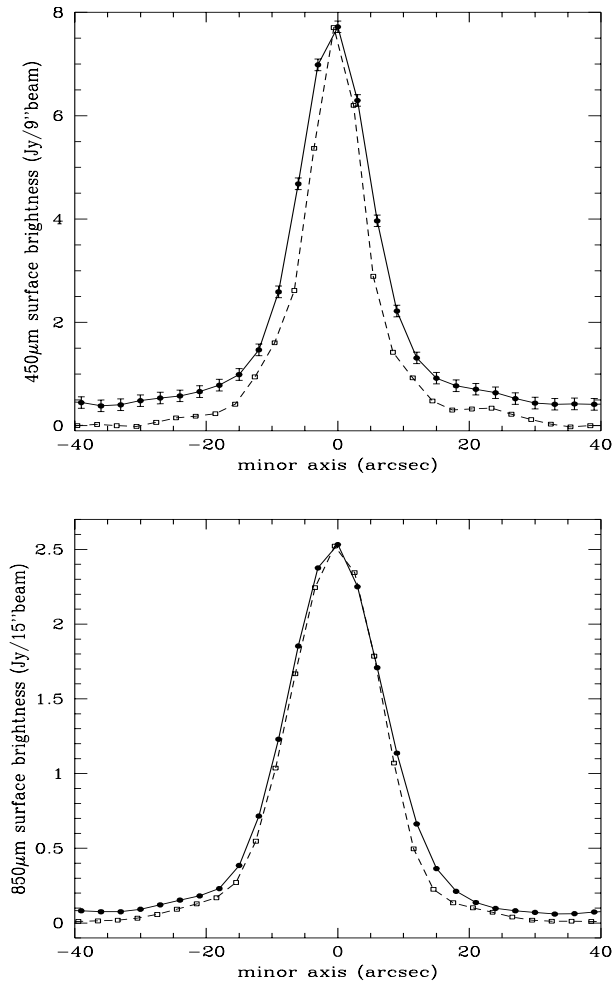


Fig. 3. Profiles along the minor axis of NGC 253 (P.A.=135°) at wavelengths of 450 μm (top) and 850 μm (bottom). In each case, the signal from the object is plotted as solid circles connected by a solid line. The corresponding beam, after normalization to the central surface brightness of the object, is denoted by the dashed line. The width of the profiles is 15'' and we use a sampling interval of 3'' along the minor axis. For both the beam profiles at 450 and 850 μm , and also for the object surface brightness at 850 μm , the errors are equal to or smaller than the size of the plotted markers.

until we inspect the 450 μm data (Fig. 2) that we infer some sort of grain expulsion along the minor axis.

In Fig. 2 we have annotated the positions of the X-ray gas and two dust filaments tentatively associated with outflow ('A' and 'B'). Filament 'A' extends in the same direction as the X-ray gas but subtends a somewhat smaller area. It is perhaps not surprising that the X-ray and submm emission do not correspond closely in shape and size for they originate from different media (X-rays arise from the bubble of ionized gas expanding directly out of the starburst whereas submm emission is expected from the neutral, dusty medium which is entrained as filaments at the superwind interface; Heckman et al. 1990). Filament 'B', situated on the diametrically opposite side of the starburst, has no counterpart at X-ray or emission-line wavelengths but *is* reminiscent of a small extension detected at 1.3mm in this direction

by Kruegel et al. (1990) (the contours in the 1.3mm map, like our own maps, are essentially elongated along the major axis, P.A. $\sim 55^\circ$, but show a slight "pinching" in the direction of the north-west half of the minor axis). A kpc-scale outflow of molecular gas has also been detected on this side of the galaxy in the 18 cm OH emission line (Turner 1985). Since the north-west side of the galaxy is closest to the observer, it is perhaps not so surprising that we do *not* detect X-ray and emission-line radiation from region 'B' (due to obscuration by gas and dust in the intervening disk). It should be stated, however, that due to NGC 253 not being completely edge-on, there remains some ambiguity as to whether filament 'B' really lies along the minor axis or is simply part of the foreground dust lane.

We emphasize, that we have checked the shape of the SCUBA beam at 450 μm and cannot attribute either of the putative filaments 'A' and 'B' to the instrumental side lobes. In fact, minor axis profiles presented in Fig. 3 show quite clearly that the features in question are many times brighter than any 'wings' we might expect from the beam and are at least 8 times above the level of the noise (they are also detected in each of the composite jiggle maps which go to make up the final 450 μm image). The de-projected distance of the minor axis submm emission from the disk of NGC 253 is 500 pc. This is slightly less, but comparable to, the size of the dust outflow in M82 (800 pc).

4. Discussion

4.1. Central starburst

One of the most noteworthy results of the IRAS mission was the recognition that a large fraction of galaxies emit the vast majority of their bolometric energy at FIR ($\sim 100 \mu\text{m}$) wavelengths as opposed to optical wavelengths (Sanders & Mirabel 1996; Soifer et al. 1987). Subsequent investigation of these 'infrared-bright galaxies' revealed that they harboured young, massive stars near the nucleus which were driving outflow along the minor axis (Armus et al. 1989; Heckman et al. 1990). The spatial correspondance between the intense FIR radiation and the newly-formed stars in these starburst galaxies has always been somewhat tenuous due to: (i) obscuration at optical wavelengths and (ii) the poor resolution capability of FIR instruments ($\sim 1'$ or ~ 1 kpc for even the closest starburst galaxies). Recently, Alton et al. (1998a) used deconvolved IRAS observations (HiRes) of the nearest edge-on galaxies to demonstrate that $\frac{3}{4}$ of the 60 μm radiation in starburst galaxies originates from an unresolved source in the inner 3 kpc of the disk. To acquire better spatial information than this usually requires going to shorter wavelengths. For example, Telesco et al. (1993) used mid-IR imaging to establish a correspondance between sites of recent star-formation and *warm* dust at the centre of FIR-bright galaxies. Similarly, Baum et al. (1993) resorted to $\sim 1''$ resolution radio continuum observations (and the previously-established FIR-radio correlation), to show that dust within FIR-bright spirals is heated primarily by circumnuclear star-formation. Indeed, this found to be true even if an active galactic nucleus (AGN) was known to be present.

Our SCUBA maps, with a resolution of $10\text{--}15''$, allow us to probe the central kiloparsec or so of these heavily obscured, starburst galaxies. Even using the submm as a tracer, we confirm that the central starburst plays an important rôle in the heating of interstellar dust. Indeed, for NGC 253 and M82, $\frac{1}{3}$ of the flux detected at $850\ \mu\text{m}$ originates from the young stars within the central 0.5 kpc. Of the remaining flux, a significant proportion arises from the dust outflow and, almost certainly, there is a contribution from young stars located at larger galactic radii. The current submm measurements are far more sensitive to cold dust rather than the kind of warm grains ($\geq 30\ \text{K}$) detected by IRAS (a 6 K blackbody has its peak emission at $850\ \mu\text{m}$). Given that the warmest grains are situated at the centre of the galaxy we would expect, therefore, that FIR imaging ($\lambda \sim 100\ \mu\text{m}$) carried out at comparable resolution to SCUBA would be almost completely dominated by the central starburst. Thus, we can confirm that, for the majority of spiral galaxies with $\frac{L_{\text{FIR}}}{L_B} \geq 1$ (selection criterion for the present observations), that the overwhelming majority of FIR energy arises from the central starburst.

Finally, we note that all the sources detected in our submm maps are clearly resolved i.e. none of the objects we have observed contains an AGN which might have somehow escaped previous detection.

4.2. Dust outflows

The submm maps presented in Fig. 1 confirm the expulsion of dust grains from the M82 starburst. They also constitute a somewhat more tentative detection of the same phenomenon in the galaxies NGC 253 and NGC 4631. In the case of NGC 4631, our observations indicate that enhanced star-formation is less centrally concentrated and that the outflow takes the form of numerous, smaller ‘chimneys’ or extra-planar filaments. NGC 4631 is very reminiscent of NGC 891 both in its FIR properties and its manifestation of a more widespread, diffuse star-forming activity (Rand 1996). NGC 891 has recently been observed at $450\ \mu\text{m}$ and $850\ \mu\text{m}$ and is known to possess a multitude of ‘dust chimneys’ which extend, like tendrils, up to 2 kpc from the midplane of the disk (Alton et al. 1998b). Although yet to be fully investigated, such behaviour has the appearance of a more localized but less energetic version of the starburst superwind.

Of the 3 objects in this study, M82 has the best resolved and most clearly identifiable dust outflow. Therefore, we adopt this object as a ‘case study’ for the purposes of the following sections. Issues we now intend to address are; (i) what is the connection between the outflowing grains and the hot superwind medium expanding along the minor axis? (ii) how much mass is contained within the outflowing grains? (iii) what is the source of the dust? (iv) what is the likelihood that expelled grains enrich the intergalactic medium?

4.2.1. Schematic model

Whilst it seems clear that the high-latitude dust in M82 has its origin somewhere in the disk (as opposed to an infall scenario which is unlikely to produce such well-defined, centrally-

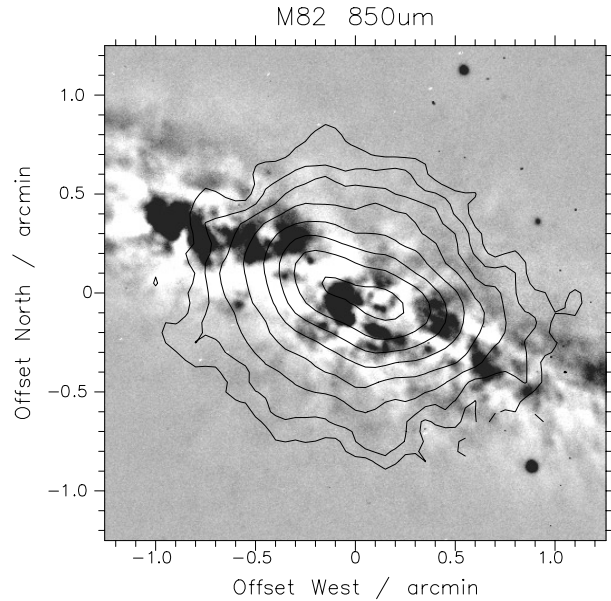


Fig. 4. Unsharp-mask B-band image of M82. The $850\ \mu\text{m}$ contours displayed in Fig. 1 are superimposed in order to compare submm emission with optical extinction features. White corresponds to the most heavily obscured regions.

located filaments), it is not obvious whether the grains in question are actually contained within the superwind fluid or are dredged up from the disk by some entrainment process. On the face of it, there is more evidence in favour of the latter scenario. In Fig. 4, we show an unsharp-masked B-band image of M82 overlaid with $850\ \mu\text{m}$ contours. Apart from dust lanes within the stellar disk (as we would expect), there is evidence from this figure for dust ‘chimneys’ extending away from the central starburst torus out along the minor axis. Although there is little detailed spatial correlation between the extraplanar submm emission and these ‘vertical’ extinction features, probably due to differences in resolution ($1''$ c.f. $15''$), there is broad agreement between these two tracers of dust. In other words, we detect submm emission from much the same region as that known to contain minor axis dust clouds. An optical colour image (B-I) by Ichikawa et al. (1994) shows that the vertical reddening lanes stretch for 1.5 kpc into the halo before arching away from the minor axis and following a path approximately parallel to the disk below. The appearance of the overall extraplanar dust structure is, therefore, one that is reminiscent of a galactic fountain. The superwind plasma, travelling at several $1000\ \text{km s}^{-1}$ (Heckman et al. 1990), appears to entrain at its working surface denser, dust-rich gas. The latter is transported some distance into the halo before being impeded by the ambient gas pressure. Within this context, the vertical B-I filaments depicted by Ichikawa et al. constitute a limb-brightening effect from a cone of dust surrounding the superwind cavity. The mass that is derived for the expelled grains (Sect. 4.2.2) is consistent with a moderately high gas density for the medium containing the grains ($\sim 10^{21}\ \text{atoms/cm}^2$), assuming that the intrinsic dust-to-gas ratio is not anomalous in some way.

Table 3. Flux densities for the dust outflow in M82. The first 4 measurements (350, 450, 750 & 850 μm) are based on the current SCUBA observations whilst the 1300, 2000 and 100 μm values are inferred from data previously published by Kruegel et al. (1990), Kuno & Matsuo (1997) and Joy et al. (1987) respectively.

Wavelength (μm)	Flux density (Jy)
350	88.4 ± 22.1
450	41.6 ± 10.4
750	4.89 ± 0.49
850	6.86 ± 0.69
1300	2.04 ± 0.41
2000	0.54 ± 0.16
100	1340 ± 67

In Fig. 5, we display the proposed entrainment model. Given that the submm emission detected along the minor axis of M82 is not solely restricted to the limb of the putative dust cone (Fig. 4), it seems probable that the entrained material resides within discrete filaments (rather than a homogeneous layer) lying along the conical working surface. Vertical extinction features detected at the centre of more face-on starburst galaxies corroborate this theory. For example, NGC 1808 is known to possess spectacular, kpc-scale dust filaments which lie along the edges of a cone with opening angle 33° (Phillips 1993). Spectroscopic studies of the minor axis confirm that a bi-conical superwind is expanding from the starburst perpendicularly out of the disk.

Although not marked in Fig. 5 we surmise that there are two potential sources for the grains accelerated out of the disk. It is possible that the dust originally flowed into the centre of the disk along a bar (known to exist in M82; Telesco et al. 1991) or the grains were, in fact, produced by massive stars in the starburst. Before examining either of these possibilities we shall first attempt to measure how much dust is present in the outflow.

4.2.2. Dust mass

Since we have observations at more than one submm wavelength we can attempt to quantify the amount of dust contained in the M82 outflow under certain assumptions about the grain emissivity. We begin by smoothing the 350, 450 and 750 μm images to the same resolution as the 850 μm data (15'' FWHM). The central torus containing the starburst has a well-defined, deconvolved size of $36'' \times 9''$ across most wavebands (Hughes et al. 1994) and, therefore, we mask this region out from all the images. It is important to integrate emission over the same area when comparing multi-wavelength observations. Therefore we use a 3σ contour on the 350 μm map, which has the poorest signal-to-noise, to define the ‘useful’ extent of the outflow. Table 3 shows the flux density contained in this region at all 4 SCUBA wavelengths.

The dust mass is most accurately determined when the temperature of the emission is tightly constrained. As far as pos-

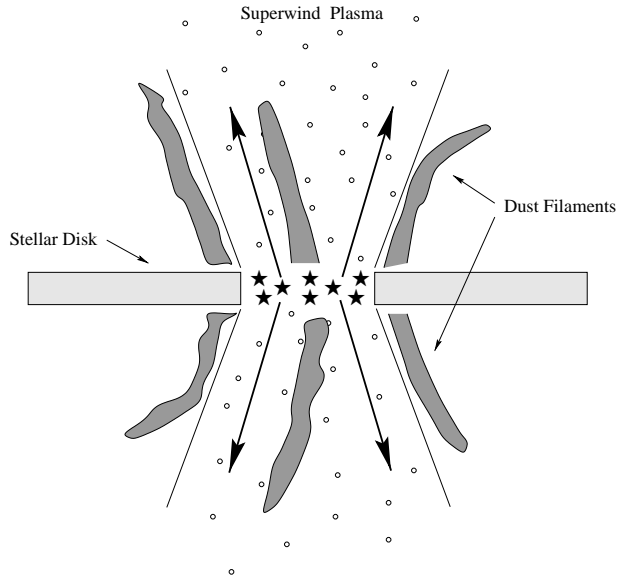


Fig. 5. Schematic model for the outflow in M82. The starburst (\star) occupies the centre of the edge-on disk. A cone of hot, ionized gas escapes in each direction along the minor axis (the superwind). As it expands, dust and gas from the disk are entrained at the working surface resulting in a network of kpc-scale filaments.

sible, therefore, we try to use previous observations of M82 in order to add further information to Table 3. At 1.3mm and 2mm respectively, Kruegel et al. (1990) and Kuno & Matsuo (1997) have detected extensions along the minor axis associated with the dust outflow. We compare the surface brightness recorded in each of their images at a distance $21''$ above and below the starburst with the corresponding values we observe at 850 μm . From the ratio of surface brightnesses we infer total flux densities of 2.04 Jy at 1.3mm and 0.54 Jy at 2mm for the region pertaining to Table 3 (this is after subtracting a contribution of 20% and 57%, respectively, due to free-free electron emission; see Hughes et al. 1990; Kuno & Matsuo 1997). Of course, a caveat to the derivation of these values is that we have assumed that there are no strong temperature gradients across the dust outflow. Similarly, a minor axis scan carried out using the Kuiper Airborne Observatory (Joy et al. 1987) offers an upper limit to the flux density at 100 μm in the outflow region (Table 3).

In Fig. 6 we have plotted the flux densities listed in Table 3 along with their associated uncertainties. We allow the spectral energy distribution to be fitted by a blackbody curve modified by $\nu \propto 1-2$ emissivity law (which is known to characterize interstellar grains in the Milky Way; Masi et al. 1995; Reach et al. 1995). The solid and dashed lines show the most extreme single-temperature fits acceptable within the observational uncertainties ($\beta=1.5$, $T=37$ K and $\beta=2$, $T=13$ K respectively). We cannot explain the deviation of the 750 μm flux density from the fit to the other points. We have re-examined both the calibration at this wavelength and the correction made for atmospheric extinction. However, we find our calibration very close to the

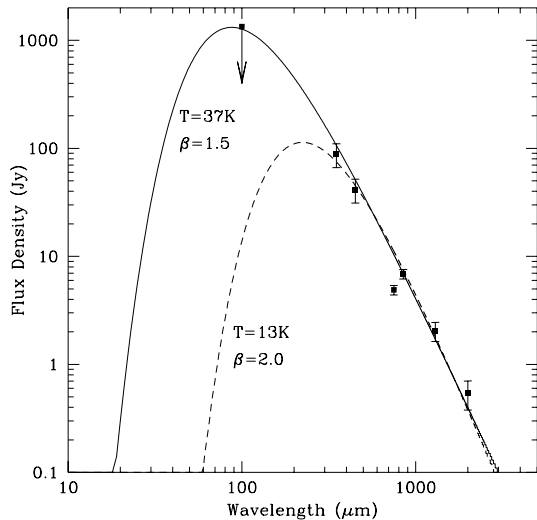


Fig. 6. Spectral energy distribution of dust along the minor axis of M82. The 350, 450, 750 and 850 μm data points come from the current SCUBA observations whilst the remainder are gleaned from the literature (see Table 3). The solid and dashed lines denote isothermal greybody fits to the data. They correspond, respectively, to the minimum and maximum dust masses which successfully reproduce the observations. We cannot explain the deviation of the 750 μm data point from the fit (see text).

canonical value and we believe that the atmospheric opacity is well determined at 750 μm .

By adopting the much-cited far infrared emissivity given by Hildebrand (1983), and using the distances listed in Table 1, we were able to derive dust masses for the isothermal fits in Fig. 6. Thus:

$$M_d = \frac{4a\rho D^2}{3} \frac{F_\nu}{Q_\nu B_{\nu,T}} \quad (1)$$

where M_d , D , a and ρ are the dust mass, galaxy distance, grain radius and grain material density respectively. F_ν , Q_ν and $B_{\nu,T}$ are the observed flux density, the grain emissivity and the value of the Planck function at the frequency ν . For the grain parameters we use the classical grain values given by Hildebrand. Thus $a = 0.1 \mu\text{m}$, $\rho = 3000 \text{kgm}^{-3}$ and:

$$Q_\nu = \frac{3}{4000} \left(\frac{\nu}{\nu_{125\mu\text{m}}} \right) \quad (2)$$

and

$$Q_\nu = \frac{3}{1300} \left(\frac{\nu}{\nu_{125\mu\text{m}}} \right)^2 \quad (3)$$

for $Q_\nu \propto 1$ and $\propto 2$ respectively (and interpolative values for intermediate power indices). Using these formulae, the implied maximum and minimum dust masses for the outflow in M82 are $1 \times 10^7 M_\odot$ and $2 \times 10^6 M_\odot$ respectively.

Our limits on the dust mass, derived from the submm/mm spectral energy distribution, span nearly an order of magnitude. The prime reason for this is that the contribution from warm grains ($T \geq 30 \text{K}$) to the long wavelength emission is poorly constrained due to an absence of data points at $< 100 \mu\text{m}$.

Furthermore, the emissivity of dust grains in the submm/mm regime (Q_ν) remains a poorly determined quantity (Hildebrand estimates a factor of 3–4 uncertainty in the values given by Eq. 2 and 3). As a matter of expedience, we turn our attention to other observations of the outflow in M82 in order to constrain the dust mass, M_d , still further. Molecular gas has been observed flowing out along the minor axis of M82 over a similar region to the grain expulsion (Nakai et al. 1987; Loiseau et al. 1990). The amount of gas associated with the outflow is estimated to be $5 \times 10^7 M_\odot$ which would imply $M_d \sim 5 \times 10^5 M_\odot$ for a solar-type dust-to-gas ratio. The high- z reddening present in the B-I colour map of Ichikawa et al (1994) can also be converted to a dust mass by assuming Milky Way type grains and a Galactic extinction law (Bohlin et al. 1978; Xilouris et al. 1997). Ichikawa et al. record dust reddening $E(B-I)=0.1-0.3$ over a 4 sq. arcmin region in the halo which accordingly suggests $M_d \sim 4 \times 10^5 M_\odot$. Notably, Phillips (1993) ascribes a similar mass to the dust outflow taking place in NGC 1808 ($M_d \sim 6 \times 10^5 M_\odot$). We emphasize that these estimates, based on reddening and outflowing molecular gas, are undoubtedly lower limits. The reddening calculations assume a foreground screen of dust and neglects photon scattering (whereas if dust and stars are mixed, M_d will be higher for the same amount of reddening due to scattering; Witt et al. 1992). For the outflowing gas we have neglected any atomic component. We conclude that the reddening/molecular gas calculations supply a lower mass limit of $10^6 M_\odot$ whilst a fit to the submm/mm photometry indicates an upper limit of $10^7 M_\odot$.

4.2.3. Origin of the ejected grains

Now that we have determined the dust mass associated with the outflow, we are in a better position to infer the origin of the expelled grains. We begin by estimating how much dust the starburst will synthesize over its lifetime. We follow Hughes et al. (1994), who have carried out a similar calculation for M82, by deriving the input of dust from massive stars ($4-16 M_\odot$) to the ISM. Within our own Galaxy (star-formation rate $\text{SFR} \simeq 4 M_\odot \text{yr}^{-1}$; Thronson et al. 1991), the collective production of dust from circumstellar shells is estimated to be $0.003-0.01 M_\odot \text{yr}^{-1}$ (Gehrz 1989; Jura 1987). Allowing for a higher SFR in M82 ($10 M_\odot \text{yr}^{-1}$; O’Connell et al. 1995) we expect the production rate in this case to be $\sim 0.015 M_\odot \text{yr}^{-1}$ (possibly somewhat more if the initial mass function is biased towards massive stars; Rieke et al. 1980). Thus, over the lifetime of the starburst ($5 \times 10^7 \text{yr}$; O’Connell et al. 1995) a total dust output of $1 \times 10^6 M_\odot$ is anticipated. This is only compatible with the *lower* limit that we have derived above for the outflowing grain material.

It is interesting to note that the dynamical timescale of the dust outflow is an order of magnitude less than the lifetime of the starburst. The velocity of the molecular gas travelling along the minor axis is believed to be 200km s^{-1} (Nakai et al. 1987). Therefore, assuming the dust is entrained in the same neutral material, the timescale for the grains to reach their present location, 800 pc above the disk, is 4×10^6 years. The corollary to this is that the dust must have built up in the disk and then subse-

quently been expelled during the last 10% of the starburst phase (it is not possible for the observed dust mass to have been synthesized by the starburst during the dynamical timescale of the outflow). Likewise, if the dust was originally transported into the centre of the disk by some sort of nonaxisymmetric gravitational stability, e.g. a bar, there must also have been some sort of ‘pile-up’ before the expulsion phase set in. The inflow rates towards the centre of starburst disks are observed to be no more than about $1 M_{\odot}$ of gas per year (Dickey 1986; Tacconi-Garman et al. 1986; Regan et al. 1997) which amounts to $\sim 10^7 M_{\odot}$ of dust over the lifetime of the bar ($\sim 10^9$ yr; Noguchi 1988; Martin & Roy 1995) but only $4 \times 10^4 M_{\odot}$ during the outflow timescale. We conclude that the outflowing grains could either have originated from the host ISM or have been synthesized by the starburst (the latter only if the lower limit to M_d is accepted) but, in either case, there must have a long-lived period of dust ‘pile-up’ around the starburst before the outflow phase set in.

4.2.4. Intergalactic enrichment

The detection of outflowing dust in starburst galaxies raises the intriguing possibility that a large number of stellar disks lose grain material and metal-rich gas to the intergalactic medium (IGM). Indeed, there is increasing evidence for diffuse dust clouds in the environment between galaxies (Masci 1998 and references therein) and, in the past, superwind galaxies have been cited as a viable source of this material (Heckman et al. 1990). In short, an intergalactic dust has been proposed to explain the apparent deficit of quasars or distant clusters seen through foreground clusters (Boyle et al. 1988; Fall & Pei 1993) and to account for the reddening of background galaxies seen through the extended halos of nearby galaxies (Zaritsky 1994). Even if the expelled grains cannot escape the gravitational well of the starburst host (and we shall attempt to answer this question presently), dust outflows are almost certain to fulfil an important rôle in the circulation of heavy elements around the disk and may explain why cold dust appears to extend beyond the stars in nearby spirals (Alton et al. 1998c; Xilouris et al. 1998; Lequeux & Guélin 1996).

The question of intergalactic enrichment hinges on whether grains are travelling fast enough to escape the gravitational field of the disk. It is important to stress at this point that, whilst the hot, ionized gas of the superwind is accelerated to velocities of several 1000 km s^{-1} (Heckman et al. 1990), both the ambient halo gas that it shocks (seen in $\text{H}\alpha$), and the dense, disk gas that it entrains, are travelling much slower (few 100 km s^{-1}). Thus, whilst the tenuous superwind fluid itself is likely to breach the halo and escape into the IGM, the fate of the entrained, neutral gas (which we believe to harbour the extraplanar grains) is less clear. Nakai et al. (1987) note that the outflow velocity of the neutral gas in M82 (200 km s^{-1}) is close to, but somewhat larger than, the corresponding escape velocity ($100\text{--}150 \text{ km s}^{-1}$). Similarly, Phillips (1993) records a deprojected velocity of $400\text{--}700 \text{ km s}^{-1}$ for the ambient material in NGC 1808 which is likely to be only marginally greater than the escape velocity of $210\text{--}530 \text{ km s}^{-1}$. Given the proximity of the outflow velocities

to the values required for escape, it is difficult to be sure about the fate of the ejected grains. Furthermore, it is possible that the high- z grains respond as much to radiation pressure (Davies et al. 1998; Norman & Ferrara 1996) as they do to gas pressure (as well as any poloidal magnetic fields that might be present; Beck et al. 1994). Within this context, the outflowing dust may decouple from the gas and its path through the halo become even more uncertain. Lastly, we note that at least some of the vertical extinction features evident in colour images of NGC 1808 and M82 appear to ‘turn over’, indicating that they might reconnect with the disk at larger galactic radii rather than escape into the IGM.

Given, hypothetically, that the outflowing grains *do* breach the halo and escape into the IGM, what contribution can we expect them to make to intergalactic enrichment? Well, we have already shown that the entrained dust mass for M82, M_d , lies between $10^6 M_{\odot}$ and $10^7 M_{\odot}$ (Sect. 4.2.2). Assuming the superwind attains a similar terminal velocity in all starburst galaxies, then the rate at which material is entrained, in the more general case, is $dM/dt \propto r_{\star}^2$ (where r_{\star} is the radial size of the central starburst; de Young 1986). Now, r_{\star} is found to scale as $L_{FIR}^{\frac{1}{2}}$, where L_{FIR} is the FIR luminosity (Heckman et al. 1990). Therefore, extrapolating from the observed dust entrained in M82, we can write for the more general case:

$$M_d = \frac{L_{FIR}}{L_{M82}} 10^{6-7} M_{\odot} \quad (4)$$

where L_{M82} is the FIR luminosity for M82 ($2 \times 10^{10} L_{\odot}$).

In an observationally important paper, Heckman et al. (1990) found that starburst-driven superwinds were associated with nearly all galaxies in the local Universe characterized by $L_{FIR} \geq L_{M82}$ and $\frac{L_{FIR}}{L_B}$ greater than unity. Although we really only have evidence for dust entrainment within the 3 examples we have observed with SCUBA (and NGC 1808, for which colour maps are available), we will assume that all galaxies possessing a superwind entrain a dust mass described by Eq. 4. The luminosity density of galaxies with $L_{FIR} \geq L_{M82}$ and $\frac{L_{FIR}}{L_B} \geq 1$ is approximately $4 \times 10^7 L_{\odot} \text{ Mpc}^{-3}$ in the local Universe (Soifer et al. 1987; Bothun et al. 1989). Thus, the amount of dust mass entrained in outflows per Mpc^3 is $2 \times 10^{3-4} M_{\odot}$. Given a space density of 0.01 Mpc^{-3} for L_{\star} galaxies (Loveday et al. 1992; de Lapparent et al. 1988), we infer a dust outflow mass of $\sim 2 \times 10^{5-6} M_{\odot}$ averaged over all spiral disks. Spiral galaxies are known to contain typically $5 \times 10^9\text{--}1 \times 10^{10} M_{\odot}$ of gas (Devereux & Young 1990). Thus, for solar-like dust-to-gas ratios (150–300; Whittet 1992), we expect to find $2 \times 10^7 M_{\odot}$ of dust in a typical disk. We conclude, therefore, that superwinds *could* be responsible for transporting 1–10% of the grains found in spiral disks up into the IGM. This conclusion, however, relies, rather speculatively, on the entrained dust having sufficient kinetic energy to leave the gravitational field of the host galaxy.

5. Summary and future observations

1. We have observed 3 nearby, edge-on, starburst galaxies using the new submm array SCUBA (operating primar-

- ily at 450 and 850 μm). These objects (M82, NGC 253, NGC 4631), are already known to possess starburst-driven superwinds and their orientation allow us to probe both the optically-obscured central starburst and any grain material escaping along the minor axis.
- For 2 of the galaxies (NGC 253 and M82), $\frac{1}{3}$ of the submm emission arises from a resolved, central source only a few hundred parsec across. This suggests that previous observations of starburst galaxies using IRAS (which is far more sensitive to the presence of warm dust), were primarily detecting emission from the starburst even though they were unable to resolve it.
 - We confirm the presence of a minor axis dust outflow in M82 and make a similar, but somewhat more tentative, report for the other two galaxies NGC 253 and NGC 4631. In all cases, the scale-size of the ‘vertical’ features is 0.7–1.2 kpc.
 - Fitting the spectral energy distribution of grains along the minor axis of M82, we infer a dust mass of $10^{6-7} M_{\odot}$. We assess the origin of these outflowing grains and conclude that they either reached the centre via a bar-type mechanism or were synthesized by massive stars within the starburst (but the latter only if the lower limit to the dust mass applies). In either case, the dust must have ‘piled up’ at the centre prior to expulsion because the outflow timescale (4×10^6 years) is too short compared with the timescale for either dust production (5×10^7 yr) or inflow ($\sim 10^9$ yr).
 - The grain outflow velocity is close to escape velocity and therefore observations of the neutral gas and dust above the disk are required to resolve the issue of whether grains enter the intergalactic medium or not. Spectropolarimetry would probably give the most direct and unequivocal indication of how the grains are moving with respect to the systemic velocity (Foley 1995). If ejected grains *do* have sufficient kinetic energy to escape the gravitational field of the host disk, we estimate that, on average, superwinds may transport up to 10% of the grains contained in spiral disks into the intergalactic medium. This value assumes that all superwind galaxies expel dust grains in a similar manner to M82 (although we have allowed for the size of the starburst by scaling according to FIR luminosity). Submm observations of a more extended sample of galaxies are needed to assess whether this is strictly true.
- Acknowledgements.* This study has benefited from discussions with several member of the SCUBA consortium – Wayne Holland, Iain Coulson, Tim Jenness and Steve Eales. We also acknowledge the use of the archival database for the Isaac Newton Group telescopes. PBA is financed by a PPARC grant.
- ## References
- Achtermann J., Lacy J., 1995, ApJ 439, 163
 Alton P., Draper P., Gledhill T., et al., 1994, MNRAS 270, 238
 Alton P., Davies J., Trewheella M., 1998a, MNRAS 296, 773
 Alton P., Bianchi S., Rand R., et al., 1998b, ApJL 507, L125
 Alton P., Trewheella M., Davies J., et al., 1998c, A&A 335, 807
 Armus L., Heckman T., Miley G., 1989, ApJ 347, 727
 Baum S., O’Dea C., Dallacassa D., de Bruyn A., Pedlar A., 1993, ApJ 419, 553
 Beck R., Carilli C., Holdaway M., Klein U., 1994, A&A 292, 409
 Bohlin R., Savage B., Drake J., 1978, ApJ 224, 132
 Bothun G., Lonsdale C., Rice W., 1989, ApJ 341, 129
 Boyle B., Fong R., Shanks T., 1988, MNRAS 231, 77
 Braine J., Kruegel E., Sievers A., Wielebinski R., 1995, A&A 295, L55
 Bregman J., Schulman E., Tomisaka K., 1995, ApJ 140, 942
 Carilli C., Holdaway M., Ho P., de Pree C., 1992, ApJ 399, L59
 Chevalier R., Clegg A., Nat 317, 44
 Davies J., Alton P., Bianchi S., 1998, MNRAS, in press
 de Jong T., Clegg P., Rowan-Robinson M., et al., 1984, ApJ 278, L67
 de Lapparent Geller M., Huchra J., 1988, ApJ 332, 44
 de Vaucouleur G., de Vaucouleurs A., Corwin H., et al., 1991, Third Reference Catalogue of Bright Galaxies
 de Young, 1986, ApJ, 307, 62
 Devereux N., Young J., 1990, ApJ 359, 42
 Dickey J., 1986, ApJ 300, 190
 Dietz R., Smith J., Hackwell J., Gehrz R., Grasdalen G., 1986, AJ 91, 758
 Donahue M., Aldering G., Stocke J., 1995, 450, L45
 Eales S., Edmunds M., 1996, MNRAS 280, 1167
 Edmunds M., 1996, In: Burkert A., Hartmann D., Majewski S. (eds.) Galactic Chemodynamics: The History of the Milky Way and its Satellite System. Astronomical Society of the Pacific
 Fabbiano G., Trinchieri G., 1984, ApJ 286, 491
 Fall S., Pei Y., 1993, ApJ 402, 479
 Foley N., 1995, Ph.D., University of Durham
 Gehrz R., 1989, IAU Sympos. 135, 445
 Heckman T., Armus L., Miley G., 1990, ApJS, 74, 833
 Heisler J., Ostriker J., 1988
 Hildebrand R., 1983, QJRAS 24, 267
 Hughes D., Gear W., Robson E., 1990, MNRAS 244, 759
 Hughes D., Gear W., Robson E., 1994, MNRAS 270, 641
 Hummel E., Dettmar R., 1990, A&A 236, 33
 Ichikawa T., van Driel W., Aoki T., et al., 1994, ApJ 433, 645
 Israel F., White G., Baas F., 1995, A&A 302, 343
 Jenness T., 1997, Starlink User Note216.1
 Joy M., Lester D., Harvey P., 1987, ApJ 319, 314
 Jura M., 1987, In: Hollenbach D., Thronson H. (eds.) Interstellar Processes 3–17. Reidel Publishing Company
 Kruegel E., Chini R., Klein U., et al., 1990, A&A 240, 232
 Leitherer C., 1993, Reviews in Modern Astronomy Vol. 7
 Lequeux J., Guelin M., 1996, In: Block D. (ed.) New Extragalactic Perspectives in the New South Africa. Kluwer, Dordrecht
 Loiseau N., Reuter H., Wielebinski R., Klein U., 1990, A&A 200, L1
 Loveday J., Peterson B., Efstathiou G., Maddox S., 1992, ApJ 390, 338
 Lynds C., Savage A., 1963, ApJ 137, 1005
 Koribalski B., Dahlem M., Mebold U., Brinks E., 1993, A&A 268, 14
 Kuno N., Matsuo H., 1997, PASJ 49, 265
 Madau P., Pozzetti L., Dickinson M., 1998, 498, 106
 Malhotra S., 1997, ApJ 488, L101
 Martin P., Roy J., 1995, ApJ 445, 161
 Masci F., 1998, in press, Publication of the Astronomical Society of Australia
 Masi S., Aquilini E., Boscaleri. A., et al., 1995, ApJ 452, 253
 Mauersberger R., Henkel C., Wielebinski R., Wiklind T., Reuter H., 1996, A&A 305, 421
 McCarthy P., Heckman T., Breugel W., 1987, AJ 92, 264
 McKeith C., Greve A., Downes P., Prada F., 1995, A&A 293, 703
 Nakai N., Hayashi M., Handa T., 1987, PASJ 39, 685

- Noguchi M., 1988, A&A 203, 259
Norman C., Ferrara A., 1996, ApJ 467, 280
O'Connell R., Gallagher J., Hunter D., Wesley C., 1995, ApJ 446, L1
Pence W., 1980, ApJ 239, 54
Phillips A., 1993, AJ 105, 486
Rand R., Kulkarni S., Hester J., 1992, 396, 97
Rand R., 1996, ApJ 462, 712
Reach W., Dwek E., Fixsen D., et al., 1995, ApJ 451, 188
Regan M., Vogel S., Teuben P., 1997, ApJ 482, L143
Rice W., 1993, AJ 105, 67
Rieke G., Lebofsky M., Thompson R., Low F., Tokunaga A., 1980, ApJ 238, 24
Rieke G., Cutri R., Black J., et al., 1985, ApJ 290, 116
Sanders D., Mirabel I., 1996, ARA&A 34, 749
Scarrott S., Eaton N., Axon D., 1991, MNRAS 252, 12p
Scarrott S., Draper P., Stockdale D., Wolstencroft R., 1993, MNRAS 264, L7
Smith P., Brand P., Puxley P., Mountain C., Nakai N., 1990, MNRAS 243, 97
Sofue Y., Wakamatsu K., Malin D., 1994, AJ 108, 2102
Soifer B., Sanders D., Madore B., et al., 1987, ApJ 320, 238
Tacconi-Garman L., Sternberg A., Eckart A., 1996, AJ 112, 918
Telesco C., 1988, ARA&A 26, 343
Telesco C., Campin H., Joy M., Dietz K., Decher R., 1991, ApJ 369, 135
Telesco C., Dressel L., Wolstencroft R., 1993, ApJ 414, 120
Thronson H., Wilton C., Ksir A., 1991, MNRAS 252, 543
Turner B., 1985, ApJ 299, 312
Wang Q., Walterbos R., Steakley M., Norman C., Robert B., 1995, ApJ 439, 176
Whittet D., 1992, Dust in the Galactic Environment. IOP Publishing
Witt A., Thronson H., Capuano J., 1992, ApJ 393, 611
Xilouris E., Kylafis N., Papamastorakis J., Paleologou E., Haerendal G., 1997, A&A 325, 135
Xilouris E., Alton P., Davies J., et al., 1998, A&A 331, 894
Zaritsky D., 1994, AJ 108, 1619